ELSEVIER

Journal of Nuclear Materials 266–269 (1999) 685–690

journal of nuclear materials

Experimental determination of the contribution of chemical sputtering of carbon on carbon core concentrations

M.F. Stamp [a,*], D. Elder [b], H.Y. Guo [a], M. von Hellermann [a], L. Horton [a], R. König [a], J. Lingertat [a], G. McCracken [a], A. Meigs [a], P. Stangeby [a,b], A. Tabasso [c]

[a] *JET Joint Undertaking, Abingdon, Oxon OX14 3EA, UK*
[b] *University of Toronto, Institute for Aerospace Studies, Ontario, Canada M3H 5TH*
[c] *Imperial College, University of London, London, UK*

Abstract

The effects of a methane puff at three different plasma locations has been compared with a similar deuterium puff in a 2.5 MA, 2.5 T Elmy H-Mode. Changes in edge and core spectroscopic signals have been examined, and show that divertor methane sources are much better screened than wall sources. The intrinsic chemically sputtered methane source from the outer divertor is derived, and shown to account for only about 15% of the carbon in the plasma core. Modelling with EDGE2D/DIVIMP, using 0.5 eV carbon atoms for the methane source, has been performed and compared with the experimental results. The model is found to correspond to the experimental trends, but it underestimates the screening of the wall methane source and overestimates the screening of methane in the divertor.

Keywords: Chemical sputtering; Carbon; Edge modeling

1. Introduction

The low Z and excellent thermal properties of graphite make it a candidate material for the first wall (and divertor target) of a tokamak reactor. However, hydrogenic bombardment of carbon causes both physical sputtering and chemical sputtering of methane and higher hydrocarbons. While the carbon physical sputtering yield [1] has a threshold energy, and can therefore be minimized by having a very low plasma edge electron temperature, the methane (CD_4) chemical sputtering yield has no threshold energy. The chemical yield depends on the surface temperature and the incident flux [2,3].

It is difficult to accurately model the transport of methane because of the absence of good molecular rate coefficients for all the dissociation pathways of CD_4 and its break-up products. We have therefore performed a series of experiments to determine the effect of a known CD_4 source on the core carbon concentrations for the JET MkIIA divertor [4].

We have also used EDGE2D/DIVIMP [5,6] to model these experiments in an attempt to judge the relative importance of the wall and divertor carbon sources, and their effectiveness in polluting the core plasma.

2. Method

The experiments were performed with a controlled CD_4 gas bleed (3×10^{21} molecules/s from 19 to 23 s) into either (i) the private flux region (PFR), (ii) the outer scrape-of-layer (SOL) or (iii) the top of the vacuum vessel (TOP), in a 2.5 MA, 2.5 T, Elmy H-mode with 12 MW of NBI. Comparison discharges were then run with a D_2 gas bleed, with the same atomic deuterium source

* Corresponding author. Tel.: +44 1235 464989; fax: +44 1235 464535; e-mail: mike.stamp@jet.uk.

0022-3115/99/$ – see front matter
PII: S0022-3115(98)00676-X

rate as the CD_4 pulse. Two types of target plasma were used, one with the strike points on the horizontal divertor tiles, and the other with the strike points on the vertical divertor tiles, Fig. 1. Gas fueling from one of the divertor valves (Fig. 1) therefore corresponds to SOL fueling or PFR fueling, depending on the strike point location. For TOP fueling, a gas valve at the top of the vacuum vessel was used with the horizontal target discharge. Note that TOP fueling is at a single toroidal location, while fueling into the divertor produces a toroidally symmetric gas input (via slits in pipes at 48 toroidal locations).

Passive visible [7], UV [8], VUV and X-ray [9,10] diagnostics were used to monitor fuel and impurity line radiation and visible bremsstrahlung, and the active charge-exchange diagnostic [11] was used to determine impurity density profiles. Fig. 1 illustrates the visible wavelength diagnostic 'outer divertor', 'inner divertor' and 'vertical' lines-of-sight that are referred to later. The UV system views part of the outer divertor with 1 cm poloidal resolution [8], whilst the VUV and X-ray systems view the plasma along near-horizontal lines-of-sight close to the plasma midplane.

The spectral line intensities (I) from neutral atoms and low charge state ions are related to particle influxes (Γ) via photon efficiencies (S/XB) through the equation [12,13]

$$\Gamma = 4\pi(S/XB)I, \tag{1}$$

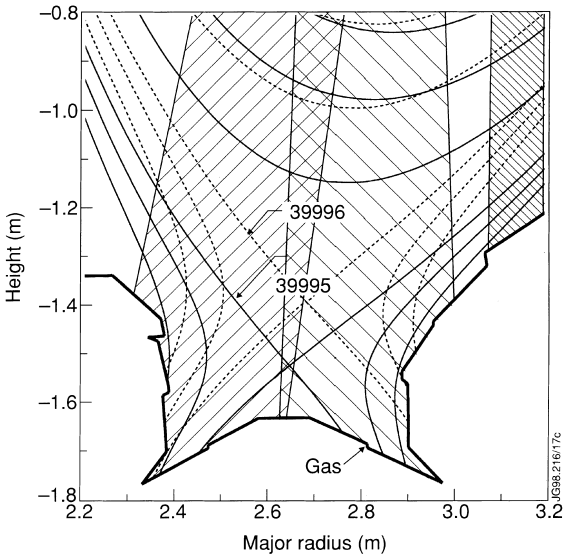

Fig. 1. X-point plasma configurations, showing the location of the divertor gas valve. SOL and TOP fueling were performed with the horizontal target configuration (#39995), and PFR fueling with the vertical target configuration (#39996). Hatched areas show the 'inner divertor', 'outer divertor' and 'vertical' (at $R = 3.1$ m) diagnostic lines-of-sight.

where S and X are the average values of the ionization and excitation rate coefficients respectively, and B the branching ratio for the observed spectral line. The photon efficiency is in general both electron temperature and electron density dependent [14,15]. The influx of methane may be derived from the intensity of the $A^2\Delta - X^2\Pi$ spectral band from one of its break-up products, CD [16,17]. Large uncertainties exist in the S/XB ratio that would convert this measured CD band intensity to the initial CD_4 influx. The production of CD molecules from the break-up of higher hydrocarbons (e.g. ethylene, ethane) is expected to be small because of the strength of the C–C bond [18].

In this paper we have taken care to match the plasma parameters in the CD_4 fueled and its comparison D_2 fueled discharge. Changes in signal intensities will then be representative of changes in influxes.

3. Experimental results

The total input power, the total radiated power (Fig. 2), the line-integral electron density (Fig. 3), the central electron and ion temperatures, the DD neutron rate, and the plasma stored energy in the TOP, SOL and PFR fueled discharge pairs were matched within 5%, with the following exceptions: (1) the electron density was 20% lower with CD_4 PFR fueling, though the outer divertor bremsstrahlung signal (523.5 nm, on the l-o-s in Fig. 1) was identical to the D_2 fueled comparison discharge. This bremsstrahlung signal is dominated by bremsstrahlung emission from the divertor, and is pro-

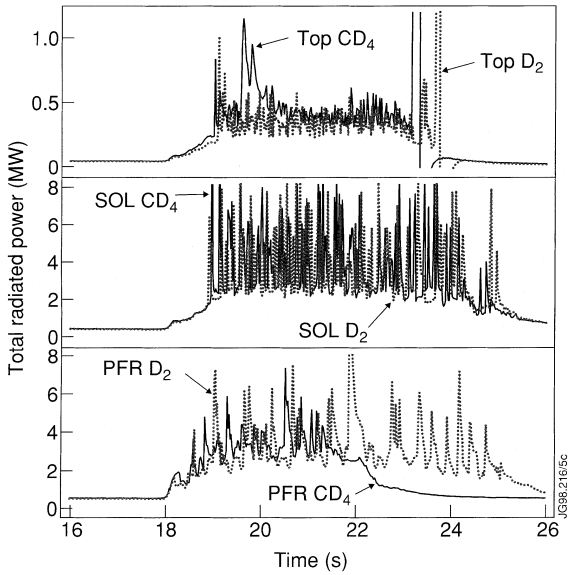

Fig. 2. Time evolution of the total radiated power for the three pairs of shots.

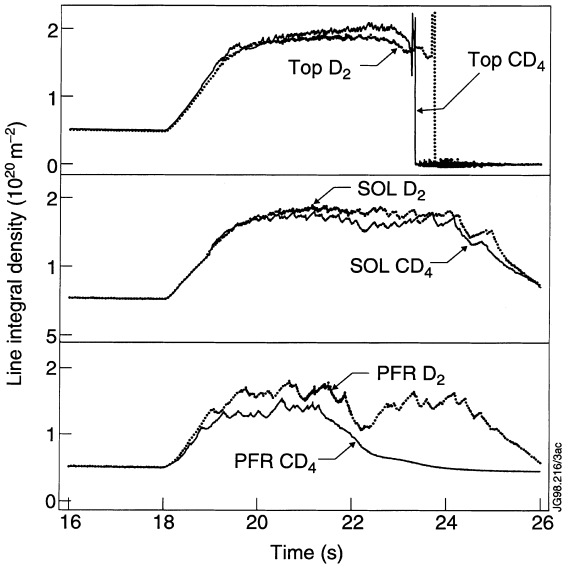

Fig. 3. Time evolution of the line integral electron density for the three pairs of shots.

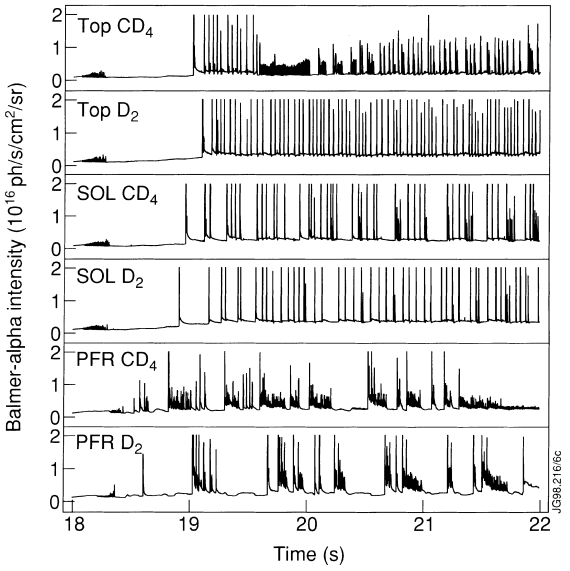

Fig. 4. Outer divertor Balmer-alpha intensity for the three pairs of shots, showing similar ELM behavior in each pair.

portional to Z_{eff} and the electron density squared, and inversely proportional to the electron temperature. The divertor electron density is therefore probably very similar in the pair of PFR discharges. (2) The total radiated power was about 10% higher with CD_4 TOP fueling and also showed the radiation spike from an inconel flake at 19.6 s. Concomitant with this extra radiation, the ELMs changed from Type I to Type III (Fig. 4). Apart from this observation, the ELM behavior in the matched discharge pairs was very similar, though the ELMs and ELM-free periods in the PFR fueled (vertical target) discharges were irregular.

We have therefore shown that the edge plasma conditions in the D_2 fueled comparison discharges were nearly identical to the CD_4 fueled discharges, and so in the following discussions we are justified in assuming that any changes in the spectroscopic signals between pairs of discharges are real changes in particle influxes.

We now look at the spectroscopic data, comparing typical between-ELM values, and start with the observations of the CD band intensity ($A^2\Delta - X^2\Pi$, 431 nm) at the inner and outer divertor, Fig. 5(a) and (b). Clearly, TOP CD_4 fueling did not change the inner or outer divertor CD signals, and outer divertor CD_4 fueling into either the SOL or PFR had little or no effect on the inner divertor CD signal, whilst doubling the outer divertor CD signal. The C III (465 nm) divertor signals followed the same trends, though the increase in signal with CD_4 fueling was only about 30%. XUV measurements of C VI (3.37 nm) on a horizontal line-of-sight showed no significant increases with either SOL or PFR CD_4 fueling, though the signals were quite noisy. Visible wavelength measurements of C VI (529 nm, $n = 7$–8) showed no change at the inner divertor for both SOL and PFR CD_4 fueling, and a small change at the outer divertor (less than about 10%).

The irregular nature of the ELMs in the PFR CD_4 and D_2 fueled discharges makes a comparison of the inner divertor CD signals (Fig. 5(a)) somewhat subjective, but there does seem to be a higher signal level during ELM-free periods in the CD_4 fueled discharge. The size of the difference is very approximately 3×10^{13} photons/s/cm^2/sr (i.e. about half the outer divertor signal change), though the edge density and temperature were very different at the inner and outer strike points, so the photon efficiencies are probably different. We conclude that some of the CD_4 puffed into the PFR near the outer strike point did manage to reach the inner divertor plasma, but that this was strongly screened because there was no observable increase in the inner divertor C III or C VI signals.

TOP fueling of CD_4 showed increased radiated power and increased main chamber C II, C III, C IV and C VI signals, with the magnitude of the increase being largest on those lines-of-sight nearest the gas valve. The wall CD signal was too weak to be observed, so it was not possible gain any information on the intrinsic wall methane source.

We now look at measurements of carbon in the plasma core. The line-integral Z_{eff} [7] at JET is derived from the line-integrated visible bremsstrahlung intensity (523.5 (±0.5) nm) from the vertical line-of-sight (Fig. 1) and the LIDAR electron temperature and electron density profiles. For these discharges Z_{eff} had a value of

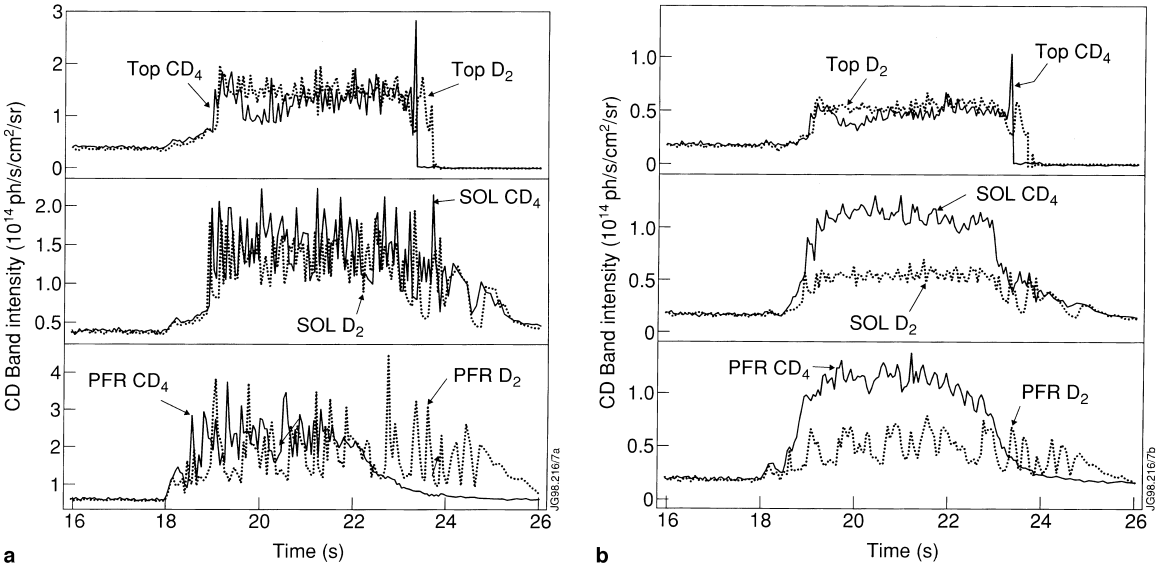

Fig. 5. (a) Comparison of the inner divertor CD band (431 nm) intensities. (b) Comparison of the outer divertor CD band (431 nm) intensities.

between 1.8 and 2.0. A less noisy Z_{eff} signal is shown in Fig. 6, where the vertical line-integrated Bremsstrahlung intensity is divided by the interferometer line-integral density squared. We can see that TOP CD_4 fueling showed a 20% increase (and a clear increase caused by the inconel flake), while both SOL and PFR fueling showed a 7% increase in Z_{eff}. Since Z_{eff} is dominated by carbon impurity, then this 7% increase in Z_{eff} is a 15% increase in the carbon concentration.

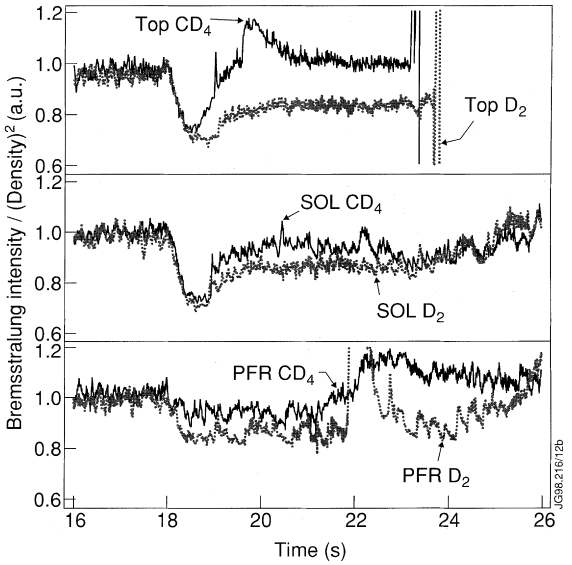

Fig. 6. Simplified Z_{eff} (Bremsstrahlung divided by density squared). The increase in Z_{eff} in #39994 due to the inconel flake at 19.6 s can be clearly seen.

Charge-exchange measurements showed that the carbon density profile and the Z_{eff} profile were hollow, with similar shapes for CD_4 and D_2 fueling. The uncertainties on the absolute carbon impurity density were rather high for these discharges, with the analysis giving a carbon density increase of about 40% for TOP CD_4 fueling, and an increase of between 0% and 20% for SOL and PFR fueling.

In summary, both SOL and PFR CD_4 fueling increased the outer divertor CD signal by 5×10^{13} photons/s/cm^2/sr (4.3×10^{19} photons/s). This increased the outer divertor C III influx by 30% and the core carbon concentration by about 15%. TOP CD4 fueling showed a larger increase in the core carbon concentration (40%), but the change in the wall CD signal was not observable.

Since the (S/XB) for CD is so uncertain, as noted earlier, it is interesting to calculate it from this experimental data. If we attribute the increase in CD signal at the outer divertor to the CD_4 fueling, then a photon efficiency of 70 methane ionizations per CD photon is derived ($T_e \sim 25$ eV, $n_e \sim 1.3 \times 10^{19}$ m^{-3} at the outer divertor). This number lies between the values calculated by Behringer [16] and Naujoks [17].

4. Modelling

We have modelled the SOL D_2 fueled discharge (#40000), using EDGE2D [5] for the plasma background solution, and DIVIMP [6] to follow the physical

and chemically sputtered carbon impurities. The particle diffusion coefficient was taken to be $D_\perp = 0.1$ m^2/s, with an inward pinch velocity, $V_{\text{pinch}} = 4.5$ m/s, and $\chi_e = 0.2$ m^2/s, $\chi_i = 0.4$ m^2/s. 'Toronto'97' chemical sputtering data [3] was used, with a yield reduction factor of 0.3 to allow for deuterium flux dependence and prompt redeposition of hydrocarbon fragments. The chemically sputtered carbon was launched by the codes as 0.5 eV carbon atoms.

The EDGE2D modelling required $P_e = 1$ MW, $P_i = 3$ MW and $n_{es} = 1 \times 10^{19}$ m^{-3} to match the J_{sat} and T_e profiles at the target plates. The divertor C II and Balmer-alpha emission profiles were also well matched, though the wall Balmer-alpha emission was underestimated by the code. This would suggest that the wall neutral pressure and the upstream separatrix density (n_{es}) were too low. Indeed, analysis by Davies et al. [19] on the relation between n_{es} and the volume average density using an 'onion-skin' model, indicates a value of 3.8×10^{19} m^{-3} for n_{es} for this discharge. This difference is under investigation. A higher separatrix density would improve the screening of impurities, but it would also increase the carbon impurity influx from the wall, so the net change is not obvious. The modelling results should therefore only be compared qualitatively with the observed trends.

Fig. 7 shows the EDGE2D/DIVIMP results for the carbon source and leakage (the amount of carbon that reaches the confined plasma) for different locations. We see that the chemically sputtered carbon source is everywhere larger than the physically sputtered source, and that the total carbon source is largest at the outer and inner divertor. The leakage plot indicates that methane produced in the divertor is almost completely screened (about 10^{-3} screening efficiency (particles reaching the core/launched particles) for the outer divertor), while wall-produced methane makes a significant contribution to core carbon (about 10^{-1} screening efficiency).

The model indicates that wall-produced carbon is contributing significantly to the core carbon, though it appears to be overestimating the screening efficiency for outer divertor (SOL) methane: From Fig. 7, doubling the outer divertor methane source would result in a 2% increase in core carbon, whereas about a 15% change was seen experimentally.

The modelling was repeated with discrete (trace) methane puffs (TOP, SOL and PFR) added to the EDGE2D plasma solution. The above conclusions were confirmed, namely that the code gave essentially no leakage from SOL and PFR methane injection, while TOP injection gave more leakage than in the experiment. On the assumption that the gas injected was large enough to be causing parallel flows, an extra parallel flow was then imposed in the DIVIMP code (running from the outer divertor round to the inner divertor). A parallel flow velocity of order 10^4 m/s was found to be sufficient to both (a) reduce the leakage for the TOP puff to about the experimental level, and (b) to increase the leakage for the SOL puff to about the experimental level.

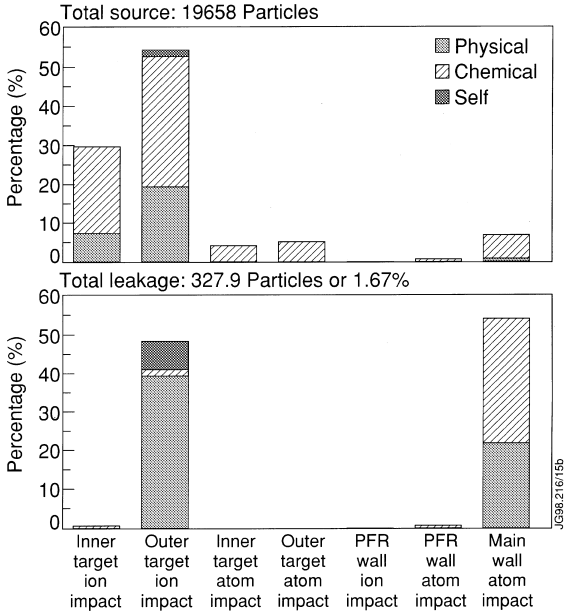

Fig. 7. EDGE2D/DIVIMP carbon source and leakage summary. The top section shows the percentage of the total source of 19,658 particles that comes from the inner target, the outer target, the PFR or the main wall via ion or atom impact. The lower section shows the same location information for the 328 particles that crossed the separatrix into the confined plasma.

5. Conclusions

Experimentally, 3×10^{21} molecules/s of TOP (i.e. wall) CD_4 fueling did not have any effect on the low charge state divertor spectroscopic signals, but did increase the core carbon density by 40%, in comparison with a D_2 fueled reference discharge. The same CD_4 source injected into either the SOL or PFR doubled the outer divertor CD signal, increased C III by 30%, and increased core carbon by about 15%, in comparison with their equivalent D_2 fueled discharges. Since the plasma edge parameters, and hence the photon efficiencies in pairs of discharges were the same, then we may conclude that the intrinsic chemically sputtered outer divertor methane source was also 3×10^{21} molecules/s, and that this contributed 15% to the core carbon density in these steady-state Elmy H-modes, assuming that CD formation from chemically sputtered higher hydrocarbons (e.g. ethane) was unimportant.

The similarity of the SOL and PFR fueling results suggests that PFR fueling is effectively screened and

does not provide any more core contamination than SOL fueling.

EDGE2D/DIVIMP modelling overestimates the screening efficiency of the outer divertor for a methane source, and underestimates the screening for a wall methane source. If, however, an additional parallel flow of order 10^4 m/s is arbitrarily added to the EDGE2D solution, then the modelling gives screening efficiencies consistent with experiment, perhaps indicative of drift effects, or puff-induced flows not included explicitly in the modelling.

The EDGE2D/DIVIMP modelling indicates that in these steady-state Elmy H-modes, the contribution of wall sources of carbon to the core carbon density are not negligible, but the poor match between the modelled and experimental wall Balmer-alpha signal prevents firmer conclusions.

References

[1] W. Eckstein et al., IPP 9/82, 1993.
[2] J. Roth, C. Garcia-Rosales, Nucl. Fusion 36 (1996) 1647.
[3] B.V. Mech, A.A. Haasz, J.W. Davies, J. Nucl. Mater. 241–243 (1997) 1147.
[4] G.C. Vlases, L. Horton, G. Matthews et al., these Proceedings.
[5] R. Simonini et al., Contrib. Plas. Physics 34 (1994) 368.
[6] P.C. Stangeby, D. Elder, Nucl. Fusion 35 (1995) 1391.
[7] P.D. Morgan et al., Rev. Sci. Instrum. 56 (1985) 862.
[8] A. Granzen, Diplomarbeit in Physik, Gerhard-Mercator University, Duisburg, 1996.
[9] R. Barnsley, K.D. Evans, N.J. Peacock, N.C. Hawkes, Rev Sci. Instrum. 57 (1986) 2159.
[10] R. Barnsley, J. Brzozowski, I.H. Coffey et al., Rev. Sci. Instr. 63 (1992) 5023.
[11] M. von Hellermann, H.P. Summers, in: R. Janev (Ed.), Atomic and Plasma Material Interaction Processes in Controlled Thermonuclear Fusion, Elsevier, Amsterdam, 1993, pp. 135–164.
[12] M.F. Stamp et al., in: Proc. of the 12th Euro. Conf. on Contr. Fusion and Plasma Phys., Budapest, vol. 9F, Part II, 1985, p. 539.
[13] K. Behringer et al., Nucl. Fusion 26 (1986) 751.
[14] K. Behringer, J. Nucl. Mater. 145–147 (1987) 145.
[15] K. Behringer et al., Plasma Phys. Contr. Fusion 31 (1989) 2059.
[16] K. Behringer, J. Nucl. Mater. 176&177 (1990) 606.
[17] D. Naujoks, these proceedings.
[18] A. Kallenbach, R. Neu, W. Poschenrieder et al., Nucl. Fusion 34 (1994) 1557.
[19] S.J. Davies, S.K. Erents et al., these Proceedings.